Open Access Journal

Journal of Power Technologies 98 (5) (2018) 387–395

journal homepage:papers.itc.pw.edu.pl

On the Combustion of Premixed Gasoline—Natural Gas Dual Fuel Blends in an Optical SI engine

Sotiris Petrakides[a,*], Daniel Butcher[b], Antonios Pezouvanis[b], Rui Chen[b]

[a] *Low Carbon Propulsion, InoMob LTD, Paphos,8020, Cyprus*
[b] *Department of Aeronautical and Automotive Engineering, Loughborough University, United Kingdom*

Abstract

Natural Gas (NG) is a promising alternative fuel. Historically, the slow burning velocity of NG poses significant challenges for its utilisation in energy efficient Spark Ignited (SI) engines. It has been experimentally observed that a binary blend of NG and gasoline has the potential to accelerate the combustion process in an SI engine, resulting in a faster combustion even in comparison to that of the base fuels. The mechanism of such effects remains unclear. In this work, an optical diagnosis has been integrated with in-cylinder pressure analysis to investigate the mechanism of flame velocity and stability with the addition of NG to gasoline in a binary Dual Fuel (DF) blend. Experiments were performed under a sweep of engine load, quantified by the engine intake Manifold Air Pressure (MAP) (0.44, 0.51. 0.61 bar) and equivalence air to fuel ratio (Φ = 0.8, 0.83, 1, 1.25). NG was added to a gasoline fuelled engine in three different energy ratios 25%, 50% and 75%. The results showed that within the flamelet combustion regime, the effect of Markstein length dominates the lean burn combustion process both from a stability and velocity prospective. The effect of the laminar burning velocity on the combustion process gradually increases as the air fuel ratio shifts from stoichiometric to fuel rich values.

Keywords: Dual Fuel; Natural Gas; Engine Combustion; Flame Stretch; Markstein Length

1. Introduction

The necessity for compliance with future emission legislations has renewed interest in the use of alternative fuels. The low carbon content, knocking resistance, and abundance reserves have classified Natural Gas (NG) as one of the most promising alternative fuels. Historically, the slow burning velocity of its main constituent, methane, has been a major concern for its utilisation in energy efficient combustion applications. The fundamental, unstretched laminar burning velocity (S_u^0) of the fuel-oxidizer mixture is often used as a major performance criterion. As emphasized in a limited body of experimental literature [1–5], a binary blend of methane and gasoline has the potential to accelerate the combustion process in an SI engine, resulting in a faster combustion even in comparison to that of the base fuels. The mechanism of such effects remains unclear.

In contrast, a substantial research effort has been made to improve the understanding of the flame behaviour of the base fuels. The combustion characteristics of NG as well as gasoline and its surrogates have been investigated both in constant volume laminar combustion experiments [6–13] as well as in SI engine environments [14–19].

In an SI engine environment, the flame is continuously stretched by its curved nature and its propagation through a strained turbulent flow field. Another fundamental mixture parameter known as the Markstein length (L_b), which quantifies the response of the flame velocity to stretch, is critically essential to completely characterise the development of an expanding flame in an SI engine.

Following the work of Karlovitz et al. [20] and Markstein [21], Clavin [22] developed a model to account for the effects of flame stretch on the development of a laminar flame. The model correlates linearly the stretched flame velocity (Sb = dRf / dt) with the unstretched laminar burning velocity (S_u^0) and the effects of stretch such as for an infinitesimally thin flame [23],

$$S_b = S_u^0 \sigma - L_b a \tag{1}$$

where σ is the expansion factor defined as the ratio of unburned to burned gas density, and a is the flame stretch rate. The flame stretch rate is an additive contributor of the aerodynamic strain and the flame curvature [20, 24, 25]. For an outwardly propagating spherical flame, and a weak effect of the tangential straining compared to the sum of normal

*Corresponding author
Email address: s.petrakides@petrakidesltd.com (Sotiris Petrakides)

straining and curvature, the global flame stretch can be simply defined as below [26, 27], where R_f is the flame radius

$$a = \frac{2}{R_f} S_b \quad (2)$$

It is clear from the definition of flame stretch that the peak value of stretch is expected at the very initial stages of combustion (small R_f). As the flame develops and flame radius increases, flame stretch is reduced.

In the context of turbulent flamelet regime, the flame front preserves the structure of a laminar flame and propagates with a stretched laminar flame velocity (S_b) [28]. The effect of turbulence on combustion is solely reduced to wrinkling of the inherently laminar flame front, increasing its surface area. Under such conditions, the effect of Markstein length (L_b) is expected to be of crucial importance to the combustion process. According to Eq. 1, for a positive/negative Markstein Length, the flame velocity will decrease/increase under flame stretch.

Constant volume laminar combustion experiments have been used throughout literature to evaluate the values of S_u^0 and L_b of a fuel-oxidizer mixture. The reported values of S_u^0 of methane is consistently lower than that of gasoline and its surrogates when tested at elevated pressures (> 2.5 bar) [7, 9, 11, 13] for all Air to Fuel Ratios (AFRs). As emphasised [9–11], these two fuels responded to flame stretch in an opposite manner with respect to the AFR. The Markstein length of iso-octane and PRF95 (95 vol% iso-octane and 5 vol% n-heptane) increases with the AFR, whereas that of methane decreases. At lean AFRs, methane has a significantly lower Markstein length compared to that of iso-octane and PRF95. It was only recently that Petrakides et al. [5, 29] and Baloo et al. [30, 31] reported values of S_u^0 and L_b for binary blends of methane with PRF95 and blends of methane with iso-octane respectively. It has been reported by Petrakides et al. [29] that for pressures relevant to SI engine operation (>5bar) and stoichiometric to lean AFRs, there is a positive synergy for blending methane to PRF95 due to the convergence of L_b of the blended fuel towards that of pure gas and S_u^0 towards that of pure liquid.

The flame behaviour of gasoline—NG DF blends has not been adequately investigated in an SI engine. There is still a limited understanding with regard to the mechanism of a faster DF flame in comparison to the base fuels in an SI engine. As stated by Aleiferis et al. [15] there is a trend of lower Markstein lengths for those fuels whose flames produced faster burning velocities in the engine environment. The aforementioned trend has been experimentally validated by the research group of Brequigny et al. [14, 32, 33].

The importance of flame-stretch interactions with the ratio of gas to liquid in a DF blend at various engine operating conditions is still a distinct research gap. The research contribution of the current experimental study is made through the characterisation and comprehensive understanding of the mechanism of DF combustion, and the importance of flame-stretch interactions under a range of engine load, and AFR, using an optically assessed research engine.

2. Experimental Methodology

2.1. Optical Research Engine

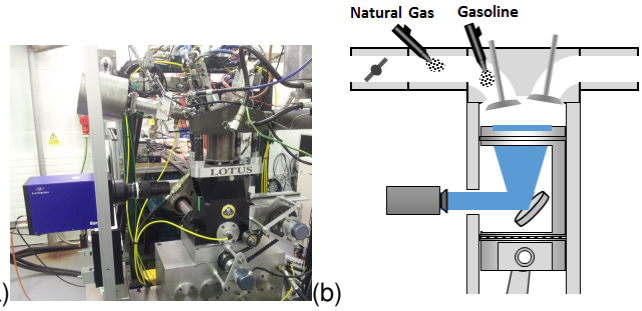

Figure 1: (a) Lotus SCORE optical research engine. (b) Optical and fuelling configurations

A single cylinder optical research engine, Lotus SCORE, is used throughout this study to allow optical measurement of the flame to be carried out. The engine is a flat piston, pent roof design with a displaced volume of 0.5 L, compression ratio of 10:1, 88 mm bore and 82.1 stroke. The engine features a centrally mounted spark plug. The configuration as shown in Fig. 1(a) is used with a cast iron cylinder liner to allow longer engine running duration in comparison to its usual fused silica liner configuration [34]. Fig. 1(b) shows how optical access is achieved through a 60 mm diameter viewing window.

Both gaseous and liquid fuels are delivered to the intake port as represented in Fig. 1(b). The liquid injector, supplied with 3.5 bar fuel, is placed closer to the cylinder to take advantage of heating from the back of the intake valve, aiding fuel vaporisation. Injection timing was 45 degree ABDC (After Bottom Dead Centre). The gas injector was a Bosch NGI-2, natural gas specific injector, supplied with 4 bar gas from a two-stage regulator via an Omega FM mass flow meter. This pressure was chosen to be within the linear operating region of the injector. The timing of both injectors, as well as ignition timing is controlled using an AVL 4210 timing unit. Unless otherwise stated, the charging duration of the ignition coil (spark dwell) was set to 1 ms.

Two data logging systems were used during the work. A low speed acquisition (1 Hz) logging intake and exhaust gas temperatures via K-type thermocouples, and liner temperature via an Omega infrared sensor. An AVL Indiset Advanced system was used to record data at crank-angle resolution including in-cylinder pressure, measured using a water-cooled Kistler 6043A60 transducer. Both were recorded using the National Instruments Labview. The AFR ratio was measured via an ECM 1200 AFR recorder, which allows H/C ratio to be adjusted as required for different fuels. The intake flow rate was recorded using a Cussons P7200 meter which has an accuracy of +/- 1%.

Optical data capture was via LaVision Nanostar intensified CCD (ICCD) camera fitted with a 105 mm Nikon UV enhanced macro lens. The CCD chip has 1280 × 1024 pixels of physical size 6.7 × 6.7 μm. In the presented work this

equates to a spatial resolution of 0.07 mm. LaVision DaVis software and the PTU9 timing unit are used for camera timing control, with inputs from the engine timing controller to allow crank angle base time to be specified.

2.2. Dual Fuel Preparation

The DF ratio is defined as the energy of NG (ENG) to the total (ETOT) energy in a DF blend as shown in Eq. 3:

$$\mathrm{DF_{Ratio}} = \frac{\mathrm{E_{NG}}}{\mathrm{E_{TOT}}} = \frac{\mathrm{E_{NG}}}{\mathrm{E_{NG}}+\mathrm{E_{Gasol.}}} = \mathrm{M_{NG}} \times \mathrm{LHV_{NG}} \qquad (3)$$

Using the measured mass flow rate of air (MAF) and natural gas (MNG), as well as the relative AFR (λ), the DF ratio was derived and displayed in real time (as well as recorded) on the AVL Indiset system. The online display of this value allows tuning of the injection duration(s) and throttle plate control to achieve the desired DF ratio at a specified engine load.

Table 1: Fuel Properties used for the derivation of DF ratio

Fuel	H/C ratio	$\mathrm{AFR_{stoich.}}$
DF100	4	17.2
DF75	3.48	16.52
DF50	3.02	15.87
DF25	2.62	15.27
DF0	1.89	14.7

The hydrogen to carbon ratio (H/C) of pure gasoline was set according to the European certification whilst its stoichiometric AFR was set to 14.7. Due to the lack of consistent data on the Lower Heating Value (LHV) of gasoline, its value was set to that of its common surrogate PRF95 (95 vol% iso-octane and 5 vol% n-heptane) and corresponds to 44.66 (MJ/kg). The LHV of methane corresponds to (50 MJ/kg). For the calculation of the stoichiometric AFR of a particular DF blend, PRF95 was used as a surrogate for gasoline and methane as a surrogate for natural gas. The stoichiometric AFR was calculated using the method of chemical balance and assuming products of complete combustion. For the different DFs, the calculated H/C ratios and stoichiometric AFRs ($\mathrm{AFR_{stoich.}}$) are summarised in Table 1, with DF100 representing pure gas (natural gas) and DF0 pure liquid (gasoline).

2.3. Engine Operating Conditions

Table 2: Experimental Test Matrix

Engine Parameter Sweep	Equivalence Ratio (Φ)	Engine Load (bar)	Fuels
AFR	0.8, 0.83, 1, 1.25	MAP:0.44	All
Load	0.8	MAP: 0.44, 0.52, 0.61	All

Two engine parameter sweeps were performed. These were MAP (controlled using throttle position), and AFR. For each sweep, the parameter under consideration was varied while the other was held constant. Engine speed was set to 2000 RPM. The experimental test matrix is summarised in Table 2.

To reveal the effect of the fuel characteristics on the combustion process, it was deemed necessary to hold the spark timing (35°CA BTDC) as well as throttle position constant for the various runs of the different DFs during the AFR, and engine load sweep. Even though a drop in volumetric efficiency is expected as DF ratio is increased, the throttle position as well as ignition timing was kept constant in order to expose all DFs to the same in-cylinder flow characteristics at the point of spark.

3. Data Processing

3.1. Thermodynamic Data

Post-processing of in-cylinder pressure data was carried out using in-house developed MATLAB code integrated with the Cantera chemical kinetics tools [35]. This allowed calculation of specific heat ratio (γ) throughout the cycle on different DF ratios. The chemical kinetics mechanism of Jerzembeck et al. [7] was used. The rate of heat release in the engine was derived with a single zone model, using the measured instantaneous in-cylinder pressure (P) and volume (V) as well as the value of the specific heat ratio (γ) of the combustible mixture as documented by Gatowski et al. [36]. For a comparison within the same engine and similar operating conditions, models representing heat transfer and blow-by are often omitted leading to Eq. 4.

$$dQ_{ch} = \frac{\gamma}{\gamma - 1} PdV + \frac{1}{\gamma - 1} VdP \qquad (4)$$

In the current study, the duration of 0-10% Mass Fraction Burned (MFB) has been used as an indication of the overall burning rate during the flame development regime, and the duration of 10-90% MFB as an indication of the overall burning rate in the developed flame regime.

3.2. Optical Data

Whilst the LaVision NanoStar is capable of acquiring 8 frames per second, timing was dictated by the engine frequency. The timing for each image was set to be a multiple of engine frequency. The timing was equivalent to 1 image every 3 cycles at 2000 RPM. The camera software, LaVision DaVis 8.1 allowed imaging at a fixed crank angle during each captured cycle. In each test condition, the software was set to step through crank angles from time of spark until TDC, taking 5 images at each crank angle before proceeding. In each test, 250 imaging engine cycles were recorded.

The derivation of the flame evolution involves the calculation of 'enflamed' areas at each crank angle. A typical chemiluminescence image is presented in Fig. 2, with a superimposed outline.

Each image was first binarised using a variable threshold, similar to the technique used by Johansson et al. [37]. A variable technique is required to account for the change

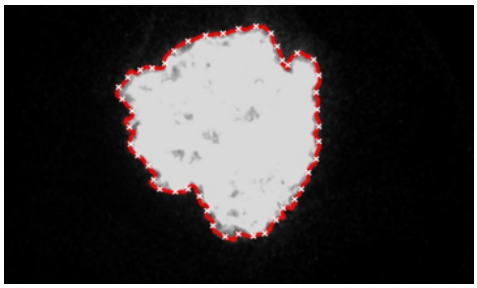

Figure 2: Performance of the Flame Detection Technique in a Typical Flame Image

in luminosity between natural gas and gasoline expanding flames.

Using the area of each binarised image, the radius of an equivalent circle is calculated; a technique used by Aleiferis et. al. [15]. The radii of each of the 5 images per crank angle are averaged to give the evolution of flame radius with crank angle. The variation statistics may also be calculated using each set of 5 radius values. The CoV (Coefficient of Variation) of this radius is a strong indicator of CoVimep within the establishment regime [38, 39].

Using the formulation of Beretta et al. [40] the MFB can be linked to the volume occupied by a flame such as,

$$MFB = \left[1 + \frac{\rho_u}{\rho_b}\left(\frac{1}{y_b} - 1\right)\right]^{-1} \quad (5)$$

where y_b is the volume fraction burned evaluated based on an equivalent sphere with the same mean flame radius, ρ_u is the unburned gas density and ρ_b the burned gas density. The ratio of unburned to burned gas density is commonly called the expansion ratio. The expansion ratio was evaluated at the point of spark for each fuel. The unburned gas temperature (T_u) was calculated using the isentropic relationship,

$$T_u = T_{IVC}\left(\frac{P}{V_{IVC}}\right)^{\frac{\gamma-1}{\gamma}} \quad (6)$$

For a particular fuel, Cantera was used to obtain both ρ_u based on the calculated temperature and measured in-cylinder pressure, as well as ρ_b through the thermodynamic equilibrium of the burned gases. The MFB in the flame establishment regime (0-5% MFB) was calculated using the optical data and Eq. 5.

4. Results

4.1. Identification of Combustion Parameters at Time of Spark

Before further discussion of the experimental work, it is useful to present the values of major combustion parameters at time of spark. These parameters will be necessary in the discussion of forthcoming sections. All relevant combustion parameters are calculated at time of spark and presented in Table 3 for a MAP of 0.44 bar and a speed of 2000 RPM.

Table 3: Combustion Parameters evaluated as spark timing

Eq. AFR (Φ)	Fuel	TSpark (K)	Abs. PSpark (bar)	σ	S_u^0 (m/s)	L_b (mm)
0.8	DF100	548	4.1	3.99	0.494	-0.12
	DF50	536	4	4.2	-	0.16
	DF0	529	3.89	4.4	0.548	0.63
1	DF100	550	4.2	4.39	0.658	0.09
	DF50	541	4.1	4.62	-	0.27
	DF0	527	3.9	4.92	0.72	0.42
1.25	DF100	553	4.2	4.31	0.523	0.19
	DF50	536	4	4.65	-	0.15
	DF0	525	3.9	5	0.649	0.12

As there is no available chemical kinetics to predict the burning velocity of the blend fuel, only the burning velocity of the base fuels was evaluated. Methane was used as a surrogate for natural gas and PRF95 as a surrogate for gasoline. The unstretched laminar burning velocity (S_u^0) of the surrogate fuels is calculated with the model of a freely propagating unstretched flame in the Cantera software package using the kinetic mechanism of Jerzemberck et al. **(author?)** [7] assuming pure fuel-air mixtures free of exhaust residuals. The kinetic mechanism used for the derivation of S_u^0 is validated against experimental values of burning velocities for both methane as well as PRF95 mixtures. As has been reported in literature [11, 41], the value of Markstein length is mainly a function of pressure, fuel and AFR. The effect of temperature and exhaust residuals can be assumed negligible compared to the mentioned contributors. Values of the Markstein length for the selected fuels have been directly used from the experimental study of the current research group [29] at an absolute pressure of 5 bar. An absolute pressure of 5 bar is very close to the pressures experienced at time of spark during the current experimental investigation, as shown in Table 3.

4.2. In-cylinder thermodynamic analysis

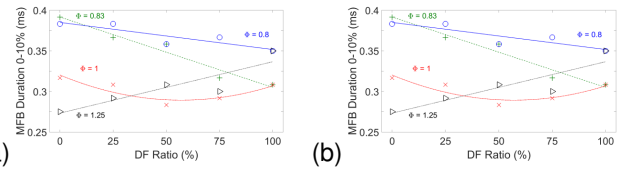

Figure 3: Burning rate in the initial (Left Plot) and developed flame regime – AFR Sweep

The duration of 0-10% MFB and 10-90% MFB was derived for all fuels and tested AFRS as illustrated in Fig. 3. It has been found that at lean conditions (Φ = 0.8, 0.83) the burning rate increased linearly with the DF ratio in both the development as well as the developed flame regime. That is evident by a linear decrease in the duration of the MFBs. At stoichiometric conditions, all DFs including natural gas are faster than gasoline in the flame development regime. However, in the developed flame regime gasoline catches up and is marginally faster than natural gas. Although all DFs are still faster than gasoline in the developed flame regime, the

differences are reduced compared to the development flame regime. Similar findings with regard to the burning rate of the base fuels at lean and stoichiometric AFRs are reported by Alreiferis et al. [42].Contrary to the lean mixtures, at a rich AFR ($\Phi = 1.25$), the burning rate is linearly decreased with DF ratio.

There is evidence that the burning rate is altered with the DF ratio. The response of burning rate with the DF ratio is contrary between lean and rich mixtures, with DFs being faster than the base fuels on stoichiometry. To reveal the mechanism behind the observed experimental phenomena, the optical data from the flame establishment regime with a parallel discussion of the fundamental combustion parameters S_u^0 and L_b are necessary.

4.3. Flame evolution analysis

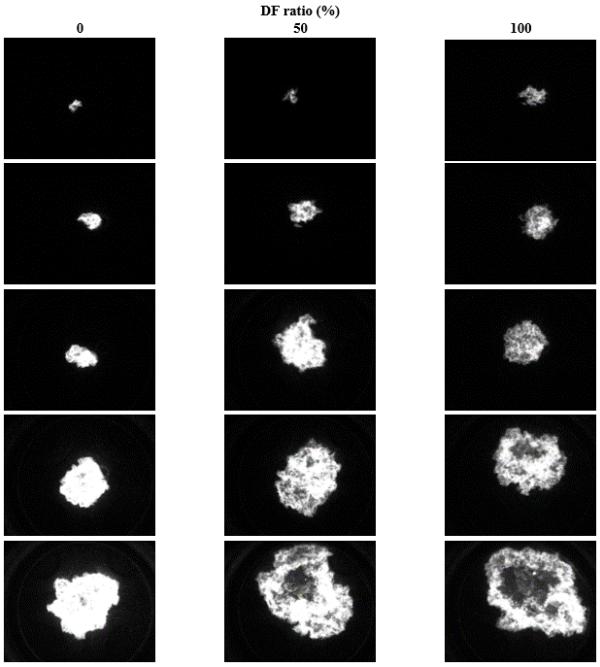

Figure 4: Typical Flame Images at 15°, 20°, 25°, and 35° CA after ignition ($\Phi = 0,8$, MAP: 0.44 bar, 2000RPM)

Fig. 4 presents a typical chronological sequence of combustion images for DF0, DF50 & DF100 at Φ = 0.8, based on the mean flame radii evolution for each test condition as illustrated in Fig. 5. As the DF ratio decreases the flame intensity appears to be higher and more spatially homogeneous. There are no luminous spots over the images and the actual flames appear reasonably circular, indicating a well-mixed fuel-air mixture absent of fuel rich zones. There is a tendency of flame development towards the upper part of the combustion chamber, where the exhaust valves are located. The phenomenon is constant for all tested conditions. It is believed to be attributed to the higher temperatures exhibited by the exhaust valves.

The mean flame radii in Fig. 5 illustrate the flame evolution of each DF blend at different AFRs. Within each subplot, the shaded region represents the period at which the

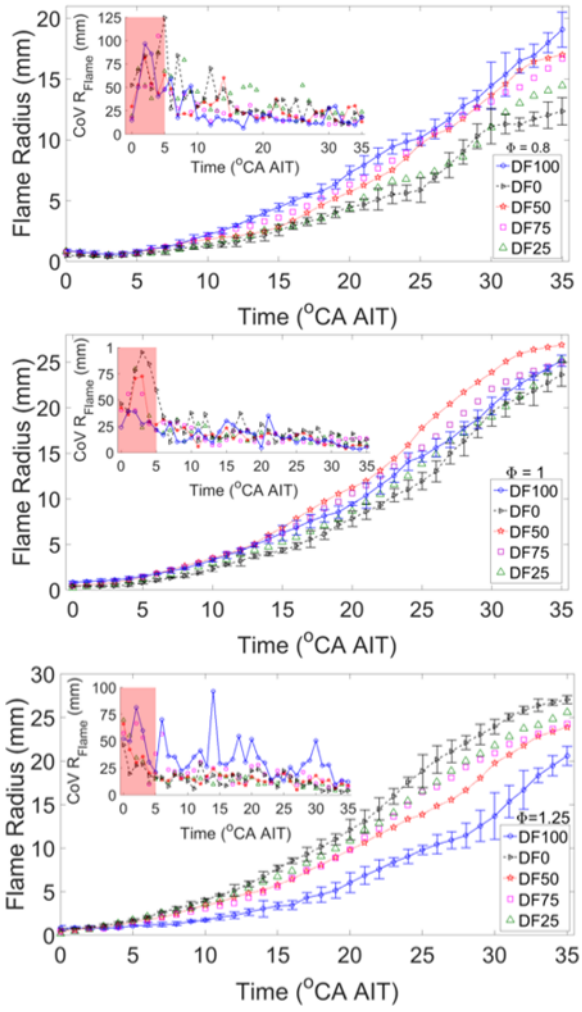

Figure 5: Flame evolution and stability at lean ($\Phi = 0,8$), stoichiometric and rich ($\Phi = 1,25$) AFRs.

spark kernel is still visible within the image. Thus, the variation of the spark kernel within this region leads to an artificially high CoV and is therefore omitted from further analysis. Further, flames with radii of greater than approximately 16 mm might not be fully visible from the optical viewing window and therefore are also removed from further analysis. These two conditions set the extremities for optical analysis of a lower boundary at 10 °CA after ignition and upper boundary of 25 °CA after ignition.

At lean conditions ($\Phi = 0.8$), even though the laminar burning velocity (S_u^0) at the point of spark is higher for gasoline compared to natural gas as shown in Table 3, the flame evolution is found to get faster as natural gas was added to gasoline, as is evident in a larger flame radius. The difference in flame radius between the base fuels is preserved through flame evolution. At stoichiometry, as the flame develops, DF50 and DF75 diverge from the flame evolution of natural gas, whereas DF25 and gasoline converge. The fastest flame evolution corresponds to DF50 and is preserved from the very early stages of combustion. At rich conditions ($\Phi = 0.8$),

and in contrast to the lean AFR, the flame evolution gets faster with the decrease of DF ratio, although DF50 and DF75 experienced very similar flame evolution.

Having illustrated and discussed the flame evolution of the various DFs in the different AFR conditions, the mechanism behind the observed phenomena can now be analysed.

4.4. The mechanism of flame behaviour

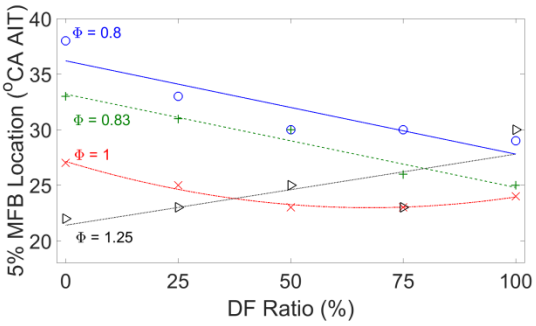

Figure 6: Burning rate versus DF ratio – AFR sweep (AIT: After Ignition Timing)

The location of 5% MFB is indicative of the burning rate at the very initial stages of combustion (flame establishment). The effect of DF ratio on the burning rate within the flame establishment regime is presented in Fig. 6.

It is apparent from Fig. 6 that in the flame establishment regime, and lean burn conditions (Φ = 0.8, 0.83), there is a linear increase in burning rate with the DF ratio (evident by a linear reduction in the 5% MFB location). The phenomena are in contrast to the fact that natural gas (DF100) has a lower burning velocity than gasoline at the point of spark as shown in Table 3. At $\Phi = 0.8$, with a 25% increase in DF ratio the burning rate increases by 8% in comparison to that of pure gasoline (DF0). At time of spark, the average absolute in-cylinder pressure is 4 bar. Under similar pressure conditions (5 bar) and $\Phi = 0.8$, the burning velocity of all DFs has been reported to be even faster than that of gasoline [29]. It is therefore evident that the burning velocity cannot explain the response of the burning rate with the DF ratio at lean burn conditions. Following Eq. 1, the other critical combustion parameter influencing the flame velocity is the Markstein length. At an absolute pressure of 5 bar and $\Phi = 0.8$, the Markstein length decreases with DF ratio [29]. Natural gas and DF50 have about 6.5 and 4 orders of magnitude lower Markstein length than gasoline respectively. It worth noting that natural gas has a negative value of L_b implying an increase of flame velocity under stretch.

In order to appreciate the effect of Markstein length on the flame velocity, a conceptual analysis was performed for the base fuels at $\Phi = 0.8$. The model described by Eq. 1, was used to derive the ratio of the stretched flame velocity to the unstretched flame velocity (Sb /Su0σ) of the base fuels. The unstretched flame velocity is defined as the burning velocity multiplied by the expansion factor. The combustion parameters at spark timing conditions as reported in Table 3 were used. To facilitate such conceptual analysis, Eq. 2 was substituted to Eq. 1 and the model was solved with respect to the stretched flame velocity such as,

$$S_b = \frac{dR_f}{d_t} = \frac{S_u^0 \sigma}{2L_b} \cdot R_f \tag{7}$$

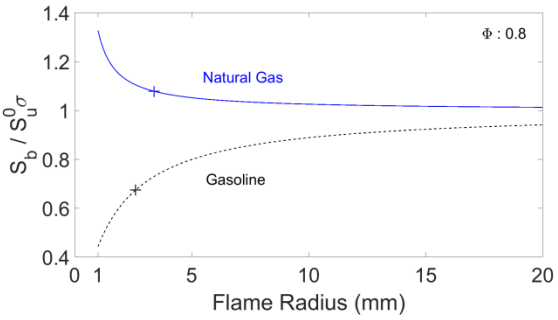

Figure 7: Conceptual Analysis of the effects of flame stretch on the flame velocity

The flame radius was iterated from 1 mm to 20 mm and the results are depicted in Fig. 7. The crosses correspond to a flame stretch of 1250 1/s. Initially, as the stretch rate experienced by the flame attains its highest value, Lb has its maximum effect on the stretched flame velocity. The stretched flame velocity of natural gas can be as much as 30% higher than its unstretched flame velocity, owing to the effect of a negative Markstein length. On the other hand, gasoline having relatively high positive values of Markstein length can experience a stretched flame velocity of less than half of its unstretched velocity.

As the flame develops and the global stretch rate is reduced, the effect of Markstein length on the flame velocity decays. However, wrinkling of the flame by turbulence will maintain the global stretch rate to a value of ~1250 1/s. In the context of the turbulent flamelet regime, the turbulent flame front propagates with a rate equal to Sb. In order to approximate the velocity of the turbulent flame front of the base fuels, the values of S_u^0 and σ are substituted in the relation Sb/$S_u^0\sigma$ at a stretch rate of 1250 1/s. The velocity of the turbulent flame front was 2 m/s for natural gas and 1.6 m/s for gasoline. The velocity of the turbulent flame front is 23% faster for natural gas than gasoline, despite its lower laminar burning velocity, owing to the value of Markstein length. The conceptual analysis reflects the mechanism of an increase in burning rate with DF ratio in lean burn conditions.

As discussed earlier, the effect of Markstein length dominates the flame propagation at lean burn conditions. In an effort to correlate the burning rate of the different DFs with their associate values of Markstein length, an extensive analysis was performed at $\Phi = 0.8$ and three different engine loads corresponding to a MAP = 0.44, 0.52, and 0.61 bar. The values of Markstein length for the different DFs, as reported in the fundamental study [29] at an absolute pressure of 5 bar, were used. The peak engine load was selected to give near 5 bar absolute pressure at the point of spark in order to be

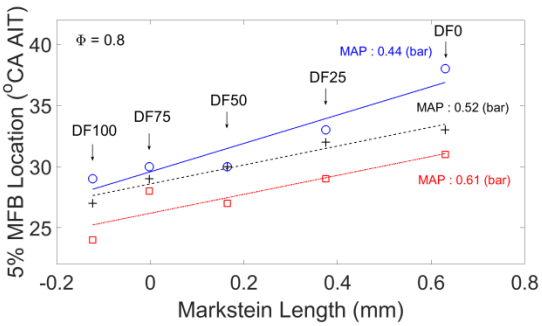

Figure 8: Correlation of burning rate with Markstein length for the engine load sweep

as close as possible to the test pressure in the fundamental study conducted by the same research group [29]. Experiments at a medium load were also performed to reveal the trend in the response of flame behaviour with an increase of in-cylinder pressure manifested by a gradual increase in engine load. For a low to high engine load, the average absolute pressure at the point of spark corresponds to 4, 4.4, and 5.1 bar. The peak in-cylinder pressures derived with pure natural gas fuelling corresponds to 10.5, 13, 18.7 bar. All experiments were performed at an engine speed of 2000 RPM. The results are illustrated in Fig. 8. At each MAP, the data are correlated with a suitable polynomial fit.

There is a strong linear correlation of the 5% MFB location and the associate value of Lb of each fuel at all tested loads. The phenomenon implies that the stretch sensitivity of the DFs is conserved from constant volume to the engine combustion and the burning rate in the flame establishment regime is governed by the value of Lb. The studies of Brequigny et al. [14, 32] under similar test conditions, reported the linear correlation of the 5% MFB with the value of of the fuel-air mixture. The Markstein length is mainly dependent on the Lewis number of the mixture, implying that the phenomena experienced in the current study are consistant with the findings of Brequigny et al. [14, 32]. Evaluated at a MAP = 0.61 bar, with a 0.2 mm decrease in L_b the burning rate is increased by 5%. The linear increase in burning rate with DF ratio, as experienced in the flame establishment regime, is preserved in the initial as well as in the developed flame regime for all test loads.

At stoichiometry ($\Phi = 1$), DF50 and DF75 experienced faster burning rates compared to the base fuels (Fig. [6]). Natural gas is faster than DF25 and, to a greater extent still, gasoline. As commented on in the previous section, the fastest flame evolution of DF50 takes place in the very initial stages of the flame establishment regime, where the flame propagates with a near laminar velocity as turbulent eddies are as yet unable to considerably affect the flame front. Experimental findings of the DFs being faster than the base fuels at Φ = 1 were also observed by the current research group in a constant volume environment under laminar conditions [29]. That was attributed to a best balance between the two fundamental combustion parameters S_u^0 and Lb which allowed for a faster flame evolution compared to the other fuels. It is therefore concluded that in the current experimental conditions, the faster burning rate of DF50 and DF75 compared to the base fuels at $\Phi = 1$, is attributed to the same mechanism.

At rich conditions ($\Phi = 1.25$), with a 25% increase in DF ratio the burning rate is decreased by 6% in the flame establishment regime (Fig. 6). As is clearly reported in the fundamental study [29], in comparison to lean conditions, as the AFR becomes richer the Markstein length of the tested fuels relatively converge to a single value, implying that S_u^0 has a higher influence on the combustion process. At $\Phi = 1.25$ as DF ratio increases S_u^0 reduces [29]. In correlation with the fundamental study, as the DF ratio increases the burning rate falls in the engine environment.

The average COV of flame radius in the range of 10 to 25 °CA after ignition was defined as the flame variability. The flame variability of all DFs at all tested AFRs is presented in Figure 9. For the base fuels and stoichiometric to lean mixtures, other relevant experimental studies have reported the CoV of the flame radius within the flame establishment regime to lie within the range of 20 to 35% [14, 17, 43].

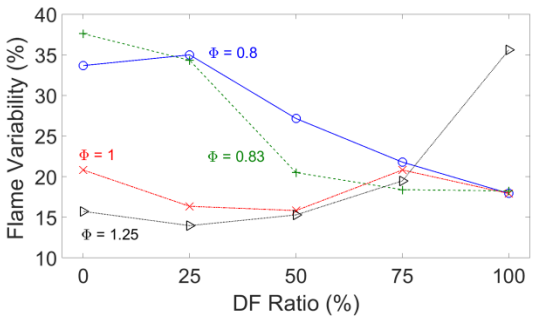

Figure 9: Flame variability – AFR Sweep

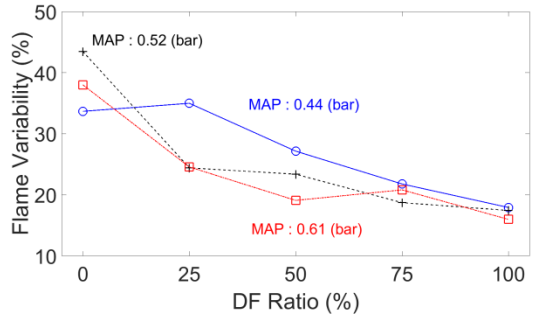

Figure 10: Flame variability—Engine load sweep

Considering the flame variability at the lean mixtures (Φ = 0.8, 0.83), there is an overall exponential decrease with the DF ratio although gasoline at $\Phi = 0.8$ deviates from the overall trend. In contrast, at $\Phi = 1.25$ there is a clear exponential increase in flame variability with the DF ratio. At stoichiometric conditions, flame variability remains relatively constant in comparison to the lean and rich conditions, with DF50 re-

sulting in the most stable flame. For all tested AFRs, there is a tendency for the fuels with the fastest burning rates in the flame establishment regime to give the lowest flame variabilities.

The flame variability at all tested engine loads is presented in Fig. [10] at $\Phi = 0.8$. An exponential decrease in flame variability with the DF ratio is clearly illustrated. The response of flame variability with the DF ratio supports the discussion in the previous section, verifying the critical influence of L_b on combustion stability under lean burn conditions. The flame variability seems to decrease with an increase in load for all DFs possible, attributed to a reduction of L_b with pressure.
While lean homogeneous operation in SI engines has previously demonstrated the ability to reduce fuel consumption and pollutant emissions [44], the degree of lean burn is limited by increasingly slow and unstable combustion. Following the discussions in the present study, the value of L_b is a dominant parameter for extending the capabilities of lean burn combustion from the perspective of both flame stability and velocity.

5. Concluding Remarks

An experimental campaign was undertaken in an optical SI engine to characterise and comprehensively understand the mechanism of gasoline-natural gas Dual Fuel (DF) combustion and the importance of flame-stretch interactions under a sweep of engine load (MAP: 0.44, 0.51. 0.61 bar), and equivalence ratio (Φ = 0.8, 0.83, 1, 1.25). Natural gas was added to gasoline in three different energy ratios: 25%, 50% and 75%. The fuels' mass burning rate is inferred from their Mass Fraction Burned (MFB) durations.

For lean burn combustion, in the flame establishment regime (0-5% MFB), at $\Phi = 0.8$, with a 25% increase in DF ratio (natural gas is added to gasoline), the burning rate increases by 8%. The effect of L_b dominates the combustion process under lean burn conditions. With a 0.2 mm decrease in L_b the burning rate increases by 5% in the flame establishment regime. The effect of L_b is preserved and dominates the combustion process in the initial (0-10% MFB) as well as in the developed (10-90% MFB) flame regime.

For lean mixtures, flame variability decreases exponentially with the increase of DF ratio. The response indicates a critical influence of L_b on combustion stability. The value of L_b is a dominant parameter for extending the capabilities of lean burn combustion, from the perspective of both flame stability and velocity.

For stoichiometric combustion, in comparison to the base fuels, DF50 and DF75 exhibit a faster burning rate in the flame establishment regime, attributed to a best balance between the two fundamental combustion parameters S_u^0 and L_b that allowed for a faster burning rate to be attained. The phenomena are still preserved in the development and developed flame regime.

For fuel rich combustion, contrary to the lean mixtures, at $\Phi = 1.25$ with a 25% increase in DF ratio the burning rate is decreased by 6%, 5% and 9% in the establishment, development and developed flame regimes respectively. In comparison to the lean mixtures, the L_b of the test fuels relatively converge to a single value, implying that S_u^0 has a critical influence on the combustion process.

To evaluate fuel performance for engine use, especially for lean burn combustion, S_u^0 is not sufficient. The value of L_b has to be primarily considered.

References

[1] M. Gou, B. Detuncq, C. Guernier, P. St-Germain, Performance of a single cylinder engine fuelled by a mixture of natural gas and gasoline, Tech. rep., SAE Technical Paper (1990).

[2] S. Di Iorio, P. Sementa, B. M. Vaglieco, Experimental investigation of a methane-gasoline dual-fuel combustion in a small displacement optical engine, Tech. rep., SAE Technical Paper (2013).

[3] S. Di Iorio, P. Sementa, B. M. Vaglieco, F. Catapano, An experimental investigation on combustion and engine performance and emissions of a methane-gasoline dual-fuel optical engine, Tech. rep., SAE Technical Paper (2014).

[4] F. Catapano, S. Di Iorio, P. Sementa, B. M. Vaglieco, Experimental analysis of a gasoline pfi-methane di dual fuel and an air assisted combustion of a transparent small displacement si engine, Tech. rep., SAE Technical Paper (2015).

[5] S. Petrakides, R. Chen, D. Gao, H. Wei, Experimental study on stoichiometric laminar flame velocities and markstein lengths of methane and prf95 dual fuels, Fuel 182 (2016) 721–731.

[6] G. Tian, R. Daniel, H. Li, H. Xu, S. Shuai, P. Richards, Laminar burning velocities of 2, 5-dimethylfuran compared with ethanol and gasoline, Energy & Fuels 24 (7) (2010) 3898–3905.

[7] S. Jerzembeck, N. Peters, P. Pepiot-Desjardins, H. Pitsch, Laminar burning velocities at high pressure for primary reference fuels and gasoline: Experimental and numerical investigation, Combustion and Flame 156 (2) (2009) 292–301.

[8] D. Bradley, R. Hicks, M. Lawes, C. Sheppard, R. Woolley, The measurement of laminar burning velocities and markstein numbers for iso-octane–air and iso-octane–n-heptane–air mixtures at elevated temperatures and pressures in an explosion bomb, Combustion and flame 115 (1-2) (1998) 126–144.

[9] O. Mannaa, M. S. Mansour, W. L. Roberts, S. H. Chung, Laminar burning velocities at elevated pressures for gasoline and gasoline surrogates associated with ron, Combustion and Flame 162 (6) (2015) 2311–2321.

[10] J. Beeckmann, O. Röhl, N. Peters, Numerical and experimental investigation of laminar burning velocities of iso-octane, ethanol and n-butanol, Tech. rep., SAE Technical Paper (2009).

[11] X. J. Gu, M. Z. Haq, M. Lawes, R. Woolley, Laminar burning velocity and markstein lengths of methane–air mixtures, Combustion and flame 121 (1-2) (2000) 41–58.

[12] G. Rozenchan, D. Zhu, C. Law, S. Tse, Outward propagation, burning velocities, and chemical effects of methane flames up to 60 atm, Proceedings of the Combustion Institute 29 (2) (2002) 1461–1470.

[13] M. Hassan, K. Aung, G. Faeth, Measured and predicted properties of laminar premixed methane/air flames at various pressures, Combustion and Flame 115 (4) (1998) 539–550.

[14] P. Brequigny, F. Halter, C. Mounaïm-Rousselle, T. Dubois, Fuel performances in spark-ignition (si) engines: Impact of flame stretch, Combustion and Flame 166 (2016) 98–112.

[15] P. Aleiferis, J. Serras-Pereira, D. Richardson, Characterisation of flame development with ethanol, butanol, iso-octane, gasoline and methane in a direct-injection spark-ignition engine, Fuel 109 (2013) 256–278.

[16] J. Serras-Pereira, P. Aleiferis, D. Richardson, An analysis of the combustion behavior of ethanol, butanol, iso-octane, gasoline, and methane in a direct-injection spark-ignition research engine, Combustion Science and Technology 185 (3) (2013) 484–513.

[17] P. G. Aleiferis, M. K. Behringer, Flame front analysis of ethanol, butanol, iso-octane and gasoline in a spark-ignition engine using laser

tomography and integral length scale measurements, Combustion and Flame 162 (12) (2015) 4533–4552.
[18] J. Sevik, M. Pamminger, T. Wallner, R. Scarcelli, R. Reese, A. Iqbal, B. Boyer, S. Wooldridge, C. Hall, S. Miers, Performance, efficiency and emissions assessment of natural gas direct injection compared to gasoline and natural gas port-fuel injection in an automotive engine, SAE International Journal of Engines 9 (2) (2016) 1130–1142.
[19] A. Catania, D. Misul, E. Spessa, A. Vassallo, Analysis of combustion parameters and their relation to operating variables and exhaust emissions in an upgraded multivalve bi-fuel cng si engine, Tech. rep., SAE Technical Paper (2004).
[20] B. Karlovitz, D. Denniston Jr, D. Knapschaefer, F. Wells, Studies on turbulent flames: A. flame propagation across velocity gradients b. turbulence measurement in flames, in: Symposium (international) on combustion, Vol. 4, Elsevier, 1953, pp. 613–620.
[21] G. Markstein, Non-steady flame propagation (1964).
[22] P. Clavin, Dynamic behavior of premixed flame fronts in laminar and turbulent flows, Progress in energy and combustion science 11 (1) (1985) 1–59.
[23] R. A. Strehlow, L. D. Savage, The concept of flame stretch, Combustion and Flame 31 (1978) 209–211.
[24] M. MATALON, On flame stretch, Combustion Science and Technology 31 (3-4) (1983) 169–181. arXiv:https://doi.org/10.1080/00102208308923638, doi:10.1080/00102208308923638.
URL https://doi.org/10.1080/00102208308923638
[25] S. Chung, C. Law, An invariant derivation of flame stretch.
[26] C. Law, C. Sung, Structure, aerodynamics, and geometry of premixed flamelets, Progress in energy and combustion science 26 (4-6) (2000) 459–505.
[27] S. Chaudhuri, A. Saha, C. K. Law, On flame–turbulence interaction in constant-pressure expanding flames, Proceedings of the Combustion Institute 35 (2) (2015) 1331–1339.
[28] A. Lipatnikov, Fundamentals of premixed turbulent combustion, CRC Press, 2012.
[29] S. Petrakides, R. Chen, D. Gao, H. Wei, Experimental investigation on the laminar burning velocities and markstein lengths of methane and prf95 dual fuels, Energy & Fuels 30 (8) (2016) 6777–6789.
[30] M. Baloo, B. M. Dariani, M. Akhlaghi, I. Chitsaz, Effect of iso-octane/methane blend on laminar burning velocity and flame instability, Fuel 144 (2015) 264–273.
[31] M. Baloo, B. M. Dariani, M. Akhlaghi, M. AghaMirsalim, Effects of pressure and temperature on laminar burning velocity and flame instability of iso-octane/methane fuel blend, Fuel 170 (2016) 235–244.
[32] P. Brequigny, F. Halter, C. Mounaïm-Rousselle, B. Moreau, T. Dubois, Thermodiffusive effect on the flame development in lean burn spark ignition engine, Tech. rep., SAE Technical Paper (2014).
[33] P. Brequigny, C. Mounaïm-Rousselle, F. Halter, B. Moreau, T. Dubois, Impact of fuel properties and flame stretch on the turbulent flame speed in spark-ignition engines, Tech. rep., SAE Technical Paper (2013).
[34] D. Butcher, A. Spencer, R. Chen, Influence of asymmetric valve strategy on large-scale and turbulent in-cylinder flows, International Journal of Engine Research (2017) 1468087417725232.
[35] D. Goodwin, H. K. Moffat, R. L. Speth, Cantera: An object-oriented software toolkit for chemical kinetics, thermodynamics, and transport processes. version 2.2. 1, Cantera Developers, Warrenville, IL.
[36] J. Gatowski, E. N. Balles, K. Chun, F. Nelson, J. Ekchian, J. B. Heywood, Heat release analysis of engine pressure data, Tech. rep., SAE Technical paper (1984).
[37] A. N. Johansson, P. Dahlander, Experimental investigation on the influence of boost on emissions and combustion in an sgdi-engine operated in stratified mode, Tech. rep., SAE Technical Paper (2015).
[38] K. Hamai, H. Kawajiri, T. Ishizuka, M. Nakai, Combustion fluctuation mechanism involving cycle-to-cycle spark ignition variation due to gas flow motion in si engines, in: Symposium (International) on Combustion, Vol. 21, Elsevier, 1988, pp. 505–512.
[39] P. G. Aleiferis, A. M. Taylor, J. H. Whitelaw, K. Ishii, Y. Urata, Cyclic variations of initial flame kernel growth in a honda vtec-e lean-burn spark-ignition engine, SAE transactions (2000) 1340–1380.
[40] G. Beretta, M. Rashidi, J. Keck, Turbulent flame propagation and combustion in spark ignition engines, Combustion and flame 52 (1983) 217–245.
[41] B. Galmiche, F. Halter, F. Foucher, Effects of high pressure, high temperature and dilution on laminar burning velocities and markstein lengths of iso-octane/air mixtures, Combustion and Flame 159 (11) (2012) 3286–3299.
[42] P. Aleiferis, J. Malcolm, A. Todd, A. Cairns, H. Hoffmann, An optical study of spray development and combustion of ethanol, iso-octane and gasoline blends in a disi engine, Tech. rep., SAE Technical Paper (2008).
[43] C. Poggiani, A. Cimarello, M. Battistoni, C. N. Grimaldi, M. A. Dal Re, M. De Cesare, Optical investigations on a multiple spark ignition system for lean engine operation, Tech. rep., SAE Technical Paper (2016).
[44] K. Nakata, N. Sasaki, A. Ota, K. Kawatake, The effect of fuel properties on thermal efficiency of advanced spark-ignition engines, International Journal of Engine Research 12 (3) (2011) 274–281.